Compact Model for Spin–Orbit Magnetic Tunnel Junctions

Mohammad Kazemi, *Student Member, IEEE*, Graham E. Rowlands, Engin Ipek, *Member, IEEE*, Robert A. Buhrman, and Eby G. Friedman, *Fellow, IEEE*

***Abstract*— Electrical control of a magnetic tunnel junction (MTJ) through spin–orbit torques (SOTs) offers opportunities to introduce MTJs into high-performance, low energy applications. SOTs support a high-speed and energy-efficient three terminal MTJ with perpendicular-to-the-plane magnetization (PMTJ). The read path is separated from the write path, enhancing the reliability of the device. SOTs exhibit two coexisting contributions: 1) a damping-like torque and 2) a field-like torque. In this paper, a physics-based compact model for a three terminal PMTJ is presented, which accurately models the magnetic, electrical, and thermal behaviors of a PMTJ controlled through SOTs. The proposed compact model is validated with experimental data, exhibiting reasonable accuracy with an average error of <5.4%. The integration capability of the proposed compact model with CMOS technology is also demonstrated.**

***Index Terms*— Compact models, damping-like spin–orbit torque (SOT), field-like SOT, three terminal magnetic tunnel junction.**

I. Introduction

ELECTRICAL control of a magnetic tunnel junction (MTJ) through spin-polarized current pulses provides opportunities to enhance speed, energy consumption, and density in a variety of applications ranging from memory [1]–[3] and logic [4] to RF oscillators [5]. Conventional two terminal MTJs are electrically controlled through spin transfer torques arising from spin-polarized current pulses with spin polarization nearly collinear with the magnetization of the free layer (FL) [6]. These torques are, therefore, initially weak, and the magnetization of the FL only gradually absorbs the energy required for switching. The time for the FL to absorb sufficient energy, referred to as the incubation time, significantly depends upon thermal fluctuations. Consequently, the device switches stochastically over a widely distributed switching time. The switching time of the conventional two terminal MTJs is on the order of several nanoseconds [6]. Hence, the device is slow and energetically inefficient due to ohmic losses during the extended period when the current pulse is applied to the device.

Current-induced spin–orbit torques (SOTs) have recently attracted considerable attention for high-performance spintronic applications operating at low energy levels [7]–[10]. Control of the magnetic configuration of an MTJ through SOTs supports a fast and energy-efficient three terminal MTJ with perpendicular-to-the-plane magnetization (PMTJ), where the read path is separated from the write path. This separation significantly enhances the reliability of the device [7], [9], [10], since the write current does not flow through tunnel barriers sensitive to electrical breakdown. Since spin polarization is nearly orthogonal to the magnetization of the FL at equilibrium states of the three terminal PMTJ, the initial SOTs are sufficiently large. Consequently, the FL is excited with an undetectable incubation time once a current pulse is applied. Deterministic and energy-efficient control of the device is, therefore, enabled, requiring short current pulses ($\leq$500 ps) [7]–[9].

An efficient compact model for an MTJ should accurately capture the device response to the applied controlling mechanism while maintaining computational efficiency. A comprehensive compact model for two terminal MTJs, known as the adaptive compact MTJ model, has recently been developed [11]. A compact model has also been proposed for three terminal PMTJs [12], [13]. Field-like and damping-like SOTs coexist within a PMTJ, and the field-like SOT may be as large as 30% of the damping-like SOT [14]. Furthermore, the magnetic and electrical responses of a PMTJ are a function of device temperature, which is characterized by Joule heating within the device [9], [15], [16]. The previously published compact model of a three terminal PMTJ [12], [13] neglects the effects of temperature on device behavior, considerably compromising model accuracy.

In this paper, a compact model is proposed for a three terminal PMTJ controlled through SOTs. The proposed compact model considers both field-like and damping-like SOTs. The model accurately captures the thermal behavior of the device and includes the effects of temperature on both the magnetic and electrical responses. The model can, therefore, be used to accurately simulate a three terminal PMTJ whose magnetic state is switched through SOTs. Furthermore, the

Manuscript received July 27, 2015; revised September 13, 2015 and October 29, 2015; accepted December 10, 2015. Date of publication January 6, 2016; date of current version January 20, 2016. The effort depicted is supported by the IARPA under Contract No. W911NF-14-C-0089. The content of the information does not necessarily reflect the position or the policy of the Government, and no official endorsement should be inferred. The review of this paper was arranged by Editor G.-H. Koh.

M. Kazemi and E. G. Friedman are with the Department of Electrical and Computer Engineering, University of Rochester, Rochester, NY 14627 USA (e-mail: mkazemi@ece.rochester.edu; friedman@ece.rochester.edu).

G. E. Rowlands and R. A. Buhrman are with the School of Applied and Engineering Physics, Cornell University, Ithaca, NY 14853 USA (e-mail: graham.rowlands@cornell.edu; rab8@cornell.edu).

E. Ipek is with the Department of Computer Science and the Department of Electrical and Computer Engineering, University of Rochester, Rochester, NY 14627 USA (e-mail: ipek@cs.rochester.edu).

Color versions of one or more of the figures in this paper are available online at http://ieeexplore.ieee.org.

Digital Object Identifier 10.1109/TED.2015.2510543

0018-9383 © 2016 IEEE. Personal use is permitted, but republication/redistribution requires IEEE permission.
See http://www.ieee.org/publications_standards/publications/rights/index.html for more information.

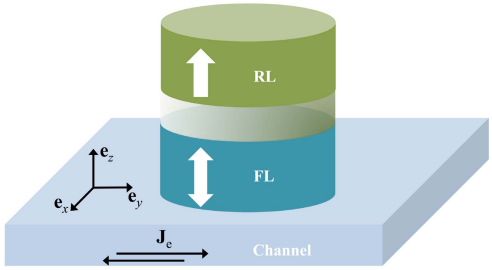

(a)

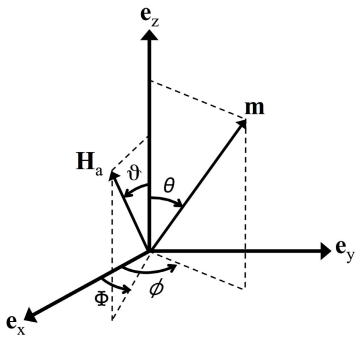

(b)

Fig. 1. Structure of a three terminal PMTJ. (a) Physical structure of the MTJ. (b) Magnetization of the FL and externally applied magnetic field. **m** denotes the unit vector along the magnetization of the FL and $\mathbf{H}_a$ is an externally applied magnetic field which assists SOTs.

model supports the analysis of a three terminal PMTJ under process variations. The capability of the model for evaluating hybrid MTJ/CMOS circuits is also illustrated through a hybrid MTJ/CMOS nonvolatile flip flop (NVFF).

The rest of this paper is organized as follows. The compact model is characterized in Section II. The model is validated with experimental data in Section III. Integration of the model with an advanced CMOS technology is shown in Section IV. Finally, some conclusions are drawn in Section V.

II. Characterization of Compact Model

The proposed compact model is based upon a modified Stoner–Wohlfarth monodomain magnetic body approximation that considers the effects of temperature on the device parameters. The proposed model captures the magnetic, electrical, and thermal behaviors of a three terminal PMTJ in response to current-induced SOTs. The compact model uses Verilog-A, a standard behavioral description language [17].

A. Structure and Operation of a Three Terminal PMTJ

A three terminal PMTJ, as shown in Fig. 1(a), is composed of two ferromagnetic (FM) layers separated by a tunneling barrier, and situated on a normal heavy metal layer, referred to as the channel. The magnetization of one FM layer, referred to as the reference layer (RL), is pinned toward the $\mathbf{e}_z$-direction, while the magnetization of the other layer, referred to as the FL, may be aligned either parallel (P) or antiparallel (AP) to the magnetization of the RL employing current-induced SOTs. Orientation of the magnetization of the FL at each time instant,

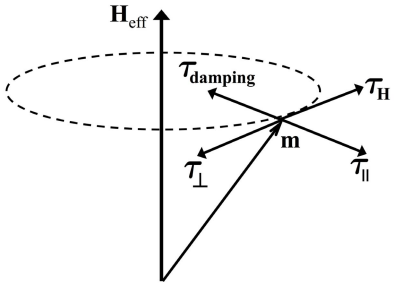

Fig. 2. Illustration of SOT components. The magnetization **m** precesses around the effective magnetic field $\mathbf{H}_{\text{eff}}$ under the influence of fields, torques, and damping effects.

as shown in Fig. 1(b), is represented by a unit vector **m** along the magnetization of the FL, which makes an angle θ with $\mathbf{e}_z$, while the plane of **m** and $\mathbf{e}_z$ makes an angle ϕ with $\mathbf{e}_x$.

B. Magnetic Response of a Three Terminal PMTJ

Temporal variation of the magnetization of the FL is governed by the Landau–Lifshitz–Gilbert (LLG)–Slonczewski equation [18],

$$\frac{d\mathbf{m}}{dt} = -\gamma\,\mathbf{m} \times \mathbf{H}_{\text{eff}} + \alpha\mathbf{m} \times \frac{d\mathbf{m}}{dt} + \gamma\,\boldsymbol{\tau}_{\text{SOT}} \tag{1}$$

where **m** is the magnetization of the FL, t is the time variable, $\mathbf{H}_{\text{eff}}$ is the effective magnetic field experienced by the magnetization of the FL, α is the Gilbert damping factor, γ is the gyromagnetic ratio, and $\boldsymbol{\tau}_{\text{SOT}}$ is the SOT composed of a damping-like SOT and a field-like SOT.

$\mathbf{H}_{\text{eff}}$ is derived from the magnetic anisotropy energies and the Zeeman energy as follows:

$$\mathbf{H}_{\text{eff}} = -\nabla_{\mathbf{m}}\left[\frac{1}{2}H_k(T)\mathbf{m}_z^2 - \mathbf{m}\cdot(\mathbf{H}_a + \mathbf{H}_d + \mathbf{H}_L)\right] \tag{2}$$

where $\mathbf{m} = (\sin(\theta)\cos(\phi), \sin(\theta)\sin(\phi), \cos(\theta))$, and $H_k(T)$ is the perpendicular-to-the-plane anisotropy field, which is a strong function of the device temperature T

$$H_k(T) = 2K_u(T)/M_s(T) - 4\pi M_s(T) \tag{3}$$

where $K_u(T)$ is the magnetic anisotropy and $M_s(T)$ is the saturation magnetization. $\mathbf{H}_a$, as shown in Fig. 1(b), is the externally applied magnetic field, and $\mathbf{H}_d$ is the magnetic field exerted by the RL. $\mathbf{H}_L = (H_{L,x}, H_{L,y}, H_{L,z})$ is the Langevin random field, which models the effect of nonzero temperature on the temporal variations of **m** [19]–[21]. Each component of $\mathbf{H}_L$ follows a zero-mean Gaussian random process whose standard deviation is a function of temperature [19]–[21]:

$$\delta = \sqrt{\frac{2\alpha k_B T}{\gamma\, M_s(T) \upsilon_{\text{FL}}}} \tag{4}$$

where parameter α is the Gilbert damping factor, γ is the gyromagnetic ratio, k_B is the Boltzmann constant, $M_s(T)$ is the saturation magnetization, υ_{FL} is the FL volume, and T denotes the device temperature governed by device self-heating. In FM thin films, the dependence of the

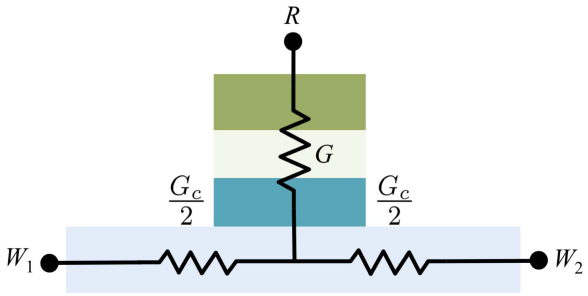

Fig. 3. Electrical model of a three terminal MTJ as a resistive $\mathbb{T}$ network.

Gilbert damping factor α on temperature T is weak, and α can be considered nearly independent of T [23].

The SOT $\boldsymbol{\tau}_{\mathrm{SOT}}$, as shown in Fig. 2, is composed of the damping-like torque ($\boldsymbol{\tau}_{\parallel}$) and field-like torque ($\boldsymbol{\tau}_{\perp}$) normal to $\boldsymbol{\tau}_{\parallel}$. Whereas $\boldsymbol{\tau}_{\perp}$ in fully metallic nanopillars is negligible, in MTJs, $\boldsymbol{\tau}_{\perp}$ can be as large as 30% of $\boldsymbol{\tau}_{\parallel}$ [14]. The choice of $\boldsymbol{\tau}_{\perp}$ must, therefore, be carefully considered in an MTJ model. Accordingly, $\boldsymbol{\tau}_{\mathrm{SOT}}$ is

$$\begin{aligned}\boldsymbol{\tau}_{\mathrm{SOT}} &= \boldsymbol{\tau}_{\parallel} + \boldsymbol{\tau}_{\perp} \\ &= \boldsymbol{\tau}_{\parallel}^{0}(\mathbf{m} \times (\sigma \times \mathbf{m})) + \boldsymbol{\tau}_{\perp}^{0}(\sigma \times \mathbf{m})\end{aligned} \tag{5}$$

where $\boldsymbol{\tau}_{\parallel}^{0}$ and $\boldsymbol{\tau}_{\perp}^{0}$ are prefactors of damping-like and field-like torques, respectively, and σ denotes the spin polarization.

In a spherical system, the coordinates (θ, ϕ) completely describe the motion of the magnetization of the FL with respect to the RL [14], [24]. Consequently, the time derivative of θ and ϕ appears independently in the LLG equation, resulting in separation of the LLG equation into two nonlinear first-order differential equations,

$$\frac{\gamma}{1+\alpha^2}\frac{d\theta}{dt} = f_\theta + \alpha f_\phi \tag{6a}$$

$$\frac{\gamma}{1+\alpha^2}\sin(\theta)\frac{d\phi}{dt} = \alpha f_\theta - f_\phi \tag{6b}$$

where α is the damping factor, γ is the gyromagnetic ratio, and both f_θ and f_ϕ are nonlinear functions of both θ and ϕ

$$\begin{aligned}f_\theta &= \boldsymbol{\tau}_{\parallel}^{0}\cos(\theta)\cos(\phi) + \boldsymbol{\tau}_{\perp}^{0}\sin(\phi) \\ &\quad - H_x\sin(\phi) + H_y\cos(\phi)\end{aligned} \tag{7a}$$

$$\begin{aligned}f_\phi &= \boldsymbol{\tau}_{\parallel}^{0}\sin(\phi) - \boldsymbol{\tau}_{\perp}^{0}\cos(\theta)\cos(\phi) \\ &\quad + (H_x\cos(\phi) + H_y\sin(\phi) - H_k\sin(\theta))\cos(\theta) \\ &\quad - H_z\sin(\theta)\end{aligned} \tag{7b}$$

where

$$\begin{aligned}H_x &= (|\mathbf{H}_a| + |\mathbf{H}_d| + |\mathbf{H}_L|)\sin(\theta)\cos(\phi) \\ H_y &= (|\mathbf{H}_a| + |\mathbf{H}_d| + |\mathbf{H}_L|)\sin(\theta)\sin(\phi) \\ H_z &= (|\mathbf{H}_a| + |\mathbf{H}_d| + |\mathbf{H}_L|)\cos(\theta)\end{aligned}$$

where $|\cdot|$ is the amplitude.

C. Electrical Response of a Three Terminal PMTJ

From a circuit point of view, a three terminal MTJ is a resistive $\mathbb{T}$ network [25], as shown in Fig. 3. G represents the tunneling conductance of the magnetic stack, and G_c represents the conductance of the channel. G comprises two components: 1) spin-independent conductance G_{SI}, which is a function of temperature and 2) spin-dependent conductance G_{SD}, which is a function of the angles enclosed by the FL and RL magnetizations (θ, ϕ) (magnetic response of the MTJ), sensing voltage V, and temperature T.

The dependence of G_{SD} on the magnetic response of the MTJ can be illustrated by the tunneling magnetoresistance (TMR) model presented in [26] and [27]. The voltage dependence of G_{SD} at zero temperature is based on the Brinkman model [28]. The temperature dependence of both the G_{SI} and G_{SD} conductances is based on the Stratton model [29]. Consequently, the tunneling conductance of the device is

$$\begin{aligned}G &= G_{\mathrm{SD}} + G_{\mathrm{SI}} \\ &= G_0\frac{\lambda T}{\sin(\lambda T)}[2 + \mathrm{TMR}(1+\cos(\theta))]\sum_{i=0}^{2} C_i V^i + \mathrm{ST}^{1.33}\end{aligned} \tag{8}$$

where G_0 is the tunneling conductance in a parallel configuration at zero temperature and zero voltage bias, and is defined as $G_0 \equiv (3.16\times10^{10}\tilde{\varphi}^{1/2}/d_b)\exp(-1.025\times\tilde{\varphi}^{1/2}d_b)$, where $\tilde{\varphi}$ is the average tunneling barrier height, and d_b is the tunneling barrier thickness. λ is a material-dependent parameter defined as $\lambda \equiv 1.387\times10^{-4}d/\tilde{\varphi}^{1/2}$, C_i, $i \in \{0,1,2\}$, is a material-dependent constant, as described in [28], and TMR denotes the TMR of the device. $\mathrm{ST}^{1.33}$ is the spin-independent conductance, where S is a fitting parameter, as described in [28], and T is the temperature.

The conductance of the channel is modeled as [9]

$$G_c = \sigma_c\frac{wd}{l} \tag{9}$$

where σ_c denotes the conductivity of the channel, l denotes the length of the channel, and w and d denote, respectively, the width and height of the channel.

D. Thermal Response of a Three Terminal PMTJ

The magnitude of the effective field experienced by the FL, as shown in (2) and (3), as well as the conductance of the device, as shown in (8), may change due to variations in device parameters caused by Joule heating. The temperature and the Joule heating effect should, therefore, be accurately considered within the compact model. Due to nonzero resistance, when the current flows into the channel, the device temperature increases through the Joule heating effect, proportional to the square of the current density [9], [15], [16]

$$T(\mathbf{J}_e) = T_0 + k|\mathbf{J}_e|^2 \tag{10}$$

where $\mathbf{J}_e$ is the current density, T_0 is the temperature at zero current density, and k is the heating rate.

The saturation magnetization M_s, magnetic anisotropy K_u, and Langevin random field $\mathbf{H}_L$ are temperature-dependent parameters that affect the effective field $\mathbf{H}_{\mathrm{eff}}$. The Langevin random field $\mathbf{H}_L$ is characterized in Section II-B. Since the device temperature remains reasonably below the Curie

temperature [16], magnetic anisotropy K_u and saturation magnetization change linearly with temperature variations [16], thus

$$M_s(T) = M_{s0}(1 - \beta(T - T_0)) \tag{11}$$

and

$$K_u(T) = K_{u0}(1 - \eta(T - T_0)) \tag{12}$$

where M_{s0} and K_{u0} are, respectively, the saturation magnetization and the magnetic anisotropy at temperature T_0. Coefficients β and η represent the change in, respectively, M_s and K_u when the temperature changes by $T - T_0$. From (10), $T - T_0 = k|\mathbf{J}_e|^2$. Hence, the saturation magnetization and the magnetic anisotropy are proportional to the square of the current density

$$M_s(T) = M_{s0}(1 - \beta k|\mathbf{J}_e|^2) \tag{13}$$

and

$$K_u(T) = K_{u0}(1 - \eta k|\mathbf{J}_e|^2). \tag{14}$$

E. Computational Complexity

As discussed in Section II-B, to compute the magnetic response of SOT-PMTJ in a computationally efficient manner, the LLG equation is separated into two simpler equations, (6a) and (6b), which are equivalent to a capacitive network with two nodes. Furthermore, since the SOT-PMTJ is a three terminal device, from an electrical point of view, the device is equivalent to a resistive network with four nodes, as shown in Fig. 3. Consequently, the proposed compact model is equivalent to an *RC* network with six nodes, which is highly computationally efficient. Nevertheless, the simulation engine that computes the compact model affects the computational time. Cadence/Spectre, which is used for evaluating the proposed compact model, provides three modes of operation: 1) conservative; 2) moderate; and 3) liberal. Moving from the liberal mode toward the conservative mode of operation provides enhanced accuracy at the expense of slightly increased computational time.

III. Model Verification

In this section, the proposed compact model is validated with experimental data. A three terminal PMTJ, controllable through SOTs, is evaluated. The compact model parameters, as listed in Table I, are based on the experimental data published in [9]. The model accurately matches the experimental data, exhibiting an average error of <5.4%.

A current pulse applied to an MTJ increases the device temperature through the Joule heating effect [9], [15], [16]. Consequently, as explained in Section II, the anisotropy decreases. As shown in Fig. 4, the model accurately captures the behavior of the device anisotropy in response to the Joule heating effect, exhibiting an average error of <1.8% and a maximum error of <5.1%.

As shown in Fig. 5(a), a switching phase diagram (SPD) of the device produced by the compact model is compared with the experimental SPD reported in [9]. The symbol "↑" means $m_z > 0$, and "↓" means $m_z < 0$. The energy profile experienced by the magnetization of the FL within a three terminal PMTJ is symmetric. The presence of a magnetic field is therefore necessary to break the symmetry, assisting SOTs to switch the magnetization of the FL. For the case of a zero magnetic field applied across the device ($\mathbf{H}_a = 0$), the magnetization of the FL does not switch to the new equilibrium state, independent of the amplitude and polarity of the current injected into the channel. For a nonzero magnetic

TABLE I
Compact Model Parameters

Parameter	Numerical value †	Description
t_{FL}	0.6×10^{-7} cm	Free layer thickness
v_{FL}	$20\mu\text{m} \times 200\mu\text{m} \times 0.6nm$	Free layer volume
l	200×10^{-4} cm	Channel length
w	20×10^{-4} cm	Channel width
d	2×10^{-7} cm	Channel thickness
M_{s0}	1.0×10^{3} emu/cm^3	Saturation mag.
K_{u0}	7.68×10^{6} erg/cm^3	Magnetic anisotropy
ρ_{FL}	5.6×10^{-6} Ωcm	Free layer resistivity
ρ_c	0.98×10^{-5} Ωcm	Channel resistivity
α	0.05	Damping factor
β	8.3×10^{-4} K^{-1}	Variation rate of M_s
η	2.2×10^{-3} K^{-1}	Variation rate of K_u
k	0.27×10^{-12}Kcm^4/A^2	Heating rate
k_B	1.38×10^{-16} erg/K	Boltzmann constant
e	1.6×10^{-19} C	Charge quantum
$\hbar$	1.05×10^{-27} ergs	Reduced Planck cons.
$\tau_{\parallel}^0$	$\zeta_{\parallel}\frac{\hbar}{2\text{eMs}t_{FL}}\mathbf{J}_e$	DL torque prefactor
$\tau_{\perp}^0$	$\zeta_{\perp}\frac{\hbar}{2\text{eMs}t_{FL}}\mathbf{J}_e$	FL torque prefactor
$\zeta_{\parallel}$	0.038	DL torque coefficient*
$\zeta_{\perp}$	0.0019	FL torque coefficient*

† Numerical value at 300 K

∗ Coefficients $\zeta_{\parallel}$ and $\zeta_{\perp}$ represent the efficiency of $\mathbf{J}_e$ in producing, respectively, damping-like (DL) and field-like (FL) torques [9].

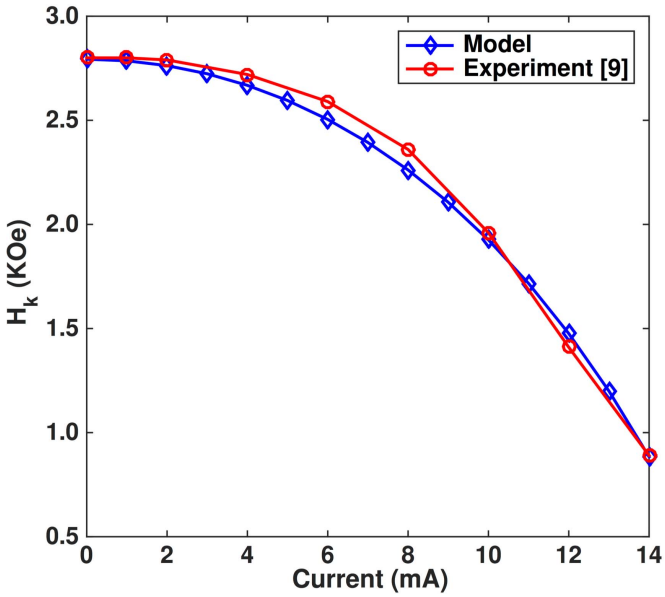

Fig. 4. H_k from the proposed compact mode as compared with the published experimental data [9]. H_k is a function of the applied current to the MTJ. The current applied to an MTJ decreases H_k through the Joule heating effect.

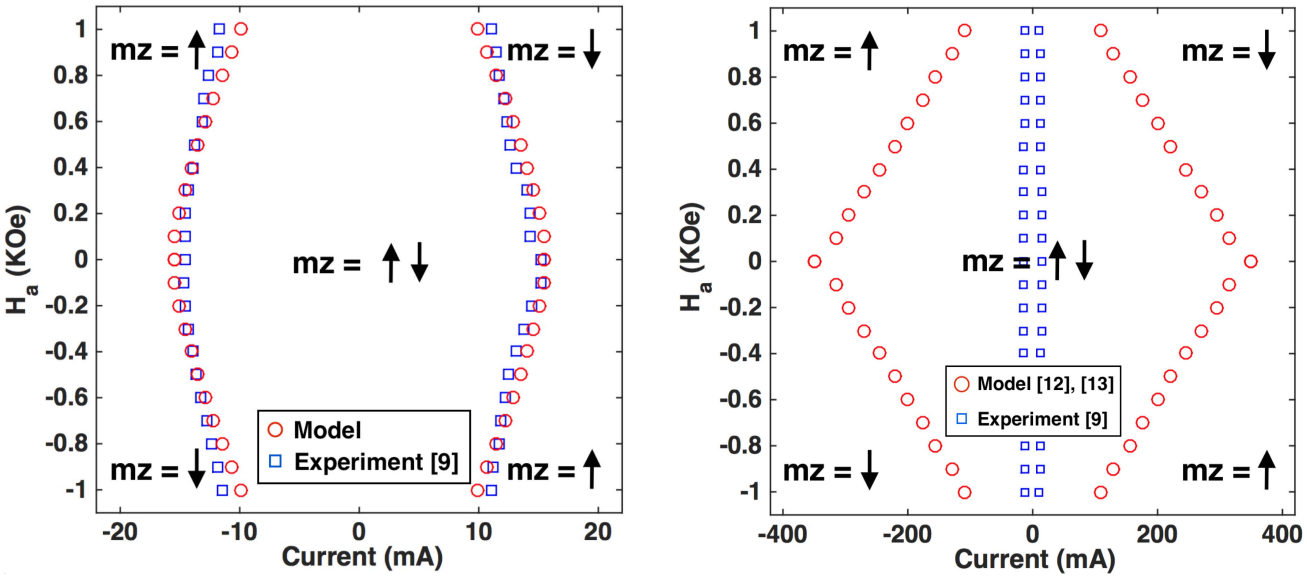

Fig. 5. SPD of the three terminal PMTJ. (a) SPD of the proposed compact model as compared with published experimental data [9]. The proposed model accurately captures the experimental data with an average error of <5.4%. (b) The SPD of the compact model in [12] and [13] as compared with published experimental data [9]. This model [12], [13] follows the general trend of the device behavior, but fails to provide sufficient accuracy.

field applied across the device along the $\mathbf{e}_y$-direction, provided that the current injected through the channel remains within the borders of the area labeled by $m_z = \uparrow\downarrow$ (see Fig. 5), the magnetization of the FL (m_z) maintains the current equilibrium state. Once the current injected through the channel passes beyond the borders of the area labeled by $m_z = \uparrow\downarrow$, the magnetization may reverse depending upon the polarity of the injected current. As shown in Fig. 5(a), the model accurately matches the experimental SPD, exhibiting an average error of less than 5.4% and a maximum error of less than 13.7%.

The current injected into the channel of a three terminal PMTJ increases the temperature of the device due to the Joule heating effect [9], [15], [16]. Furthermore, as discussed in Sections II and III, the parameters of a three terminal PMTJ are highly temperature dependent [9], [15], [16]. Hence, both the magnetic and electrical responses of a three terminal PMTJ are a function of the device temperature or, equivalently, the current density injected into the channel. The previously published compact model for a three terminal PMTJ [12], [13] does not consider the temperature dependence of the device parameters or the variation of the device temperature due to the Joule heating effect. Consequently, although the existing model produces the general trend of the device behavior, this model fails to provide sufficient accuracy, as shown in Fig. 5(b).

IV. Hybrid MTJ-CMOS Simulation Capability

The integration capability of the compact model with an advanced CMOS technology [25] is demonstrated in this section through the evaluation of an NVFF. As shown in Fig. 6, three terminal PMTJs are incorporated into a CMOS flip flop to enable nonvolatility. Introducing nonvolatility into a CMOS

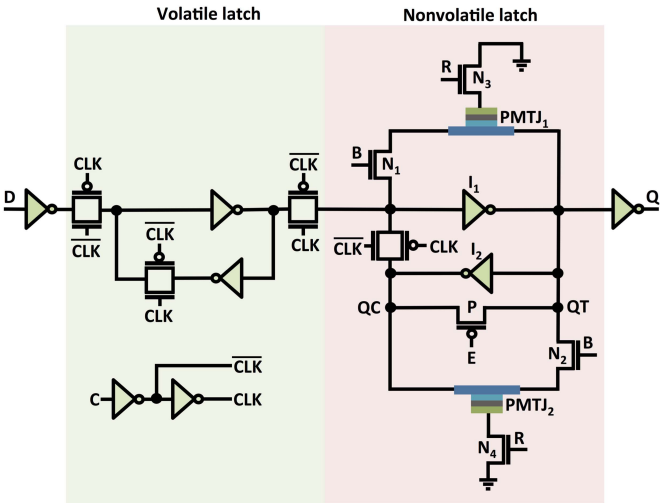

Fig. 6. NVFF based on three terminal PMTJs composed of a volatile master latch followed by a nonvolatile slave latch.

flip flop using two or three terminal PMTJs is a promising technique [31]–[34] to preserve data when a power gating (PG) domain is turned OFF. During active mode, an NVFF operates as a conventional CMOS flip flop. An NVFF stores the logic state within PMTJs once the backup mode is initiated. During sleep mode, where the PG domain is disconnected from the power supply, an NVFF retains the logic state within the PMTJs. When the active mode is initiated, the stored logic state is retrieved from the NVFF, and the PG domain resumes normal operation.

The NVFF is composed of a volatile master latch followed by a nonvolatile slave latch. The nonvolatile latch includes two PMTJs (PMTJ1 and PMTJ2) that retain the latched bit when the circuit is powered OFF. As shown in Fig. 6, each

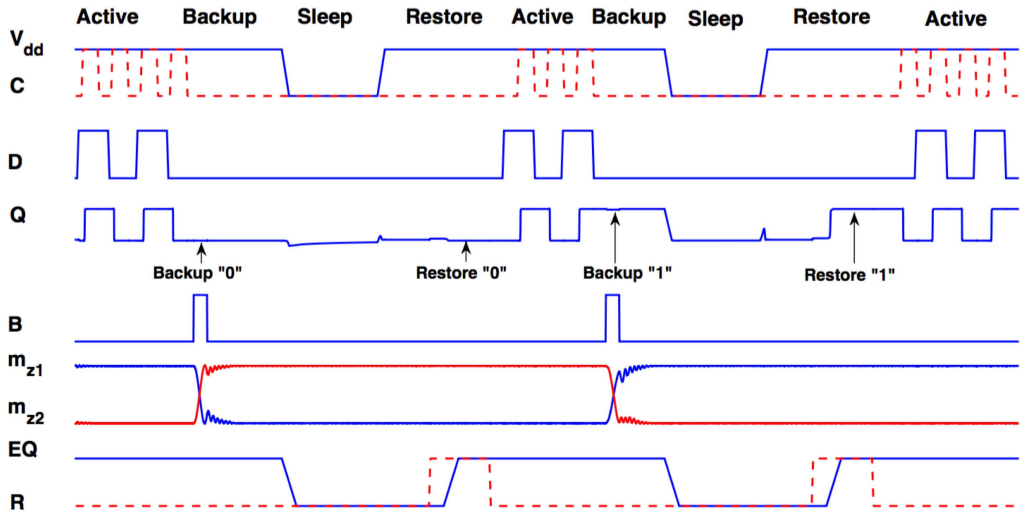

Fig. 7. Timing diagram of NVFF based on three terminal PMTJs composed of a volatile master latch followed by a nonvolatile slave latch. Both the 0 and 1 states can be stored before power is gated OFF. The stored state is restored after the sleep mode of operation is ended and the active mode is reentered.

TABLE II
NVFF SIMULATION PARAMETERS

Component		Value	Description
Transistors	P	8 / 20	No. of fins / length (nm)
	N_1, N_2	2 / 28, 2 / 32	No. of fins / length (nm)
	Other P-type FinFETs	6 / 20	No. of fins / length (nm)
	Other N-type FinFETs	4 / 20	No. of fins / length (nm)
PMTJs	Channel size	150 / 100 / 2	Length / width / thickness (nm)
	Free layer size	100 / 100 / 1	Length / width / thickness (nm)
V_{dd}		0.8	Supply voltage (V)
B pulse duration		300	Backup time (ps)
R pulse duration		1.2	Restore time (ns)

PMTJ is accessible through two nMOS transistors. The timing diagram shown in Fig. 7 illustrates the process in which signals B, R, and E, are sequenced to perform different modes of operation, i.e., active, backup, sleep, and restore. Simulation of the NVFF is performed within the Cadence/Spectre environment, and uses the proposed compact model of a three terminal PMTJ and an industrial model for a 14-nm FinFet CMOS technology [30]. The simulation parameters are listed in Table II.

The NVFF behaves as a conventional flip flop during the active mode of operation, where signals B and R are held low and signal E is held high to make the PMTJs inaccessible. Neither PMTJ switches the state.

As discussed in Sections II and III and experimentally demonstrated in [9], [15], and [16], Joule heating caused by a current pulse injected into the channel produces switching at lower current amplitudes. The proposed compact model considers the effects of temperature on the behavior of the SOT-PMTJs, accurately capturing the experimental data. A current pulse with an amplitude of 38 μA and a duration of 300 ps is sufficient to switch the PMTJs within the NVFF, performing the backup operation. This current can be provided by the cross-coupled inverters, I_1 and I_2, within the slave latch. Therefore, in contrast to the circuit proposed in [30], dedicated write drivers are not required, resulting in a more efficient circuit.

To backup the latched bit by storing the bit within the PMTJs before gating $V_{\rm dd}$ OFF, the B signal is asserted high and the C signal is held low. Once the B signal is high, a current flows through the channel of both PMTJs due to the voltage difference between QC and QT. When QC is high and QT is low, inverter I_1 sources current and inverter I_2 sinks current, changing the magnetization of the FL of $\rm PMTJ_1$ and $\rm PMTJ_2$ to, respectively, P and AP states. When QC is low and QT is high, inverter I_1 sinks current and inverter I_2 sources current, causing the magnetization of the FL of $\rm PMTJ_1$ and $\rm PMTJ_2$ to switch, respectively, to the AP and P states.

The data restore operation is performed when the flip flop is enabled to resume conventional operation. The restore operation relies on the different current drive capabilities of $\rm PMTJ_1$ and $\rm PMTJ_2$. More specifically, during the data restore operation, $\rm PMTJ_1$ and $\rm PMTJ_2$ are at different magnetic configurations, exhibiting different electrical resistances. To perform the restore operation, as shown in Fig. 7, power supply $V_{\rm dd}$ is turned ON, and C and E are initially held low. Sweeping the power from 0 to $V_{\rm dd}$ charges the parasitic capacitance at storage nodes QC and QT through the p channel path of inverters I_1 and I_2. QC and QT simultaneously discharge, respectively, through $\rm PMTJ_1$ and $\rm PMTJ_2$. If, for instance, the stored bit is 1, $\rm PMTJ_1$ is in the P state and $\rm PMTJ_2$ is in the AP state. The current drive of $\rm PMTJ_2$ is, therefore,

weaker than $PMTJ_1$, resulting in QC more slowly discharging than QT, establishing $V_{QC} > V_{QT}$. Due to the positive feedback, the regenerative action is enabled through the cross-coupled inverters, settling V_{QC}, V_{QT}, and V_Q to, respectively, V_{dd}, 0, and V_{dd}, as shown in Fig. 7.

V. Conclusion

A new compact model is described for three terminal perpendicular-anisotropy MTJs (PMTJs) composed of two ferromagnetic layers separated by a tunneling barrier and placed on a normal heavy metal with strong spin–orbit coupling. The proposed model captures the magnetic, electrical, and thermal behaviors of a three terminal PMTJ in response to SOTs. The proposed compact model considers the effects of both damping-like and field-like SOTs on device behavior. The model also considers the dynamic behavior of the self-heating process within the device. The compact model is validated using published experimental data, showing reasonably accurate results with an average error of <5.4%. The integration capability of the compact model with an advanced CMOS technology is demonstrated through the simulation of a non-volatile flip flop composed of both transistors and three terminal PMTJs.

References

[1] E. Chen *et al.*, "Advances and future prospects of spin-transfer torque random access memory," *IEEE Trans. Magn.*, vol. 46, no. 6, pp. 1873–1878, Jun. 2010.

[2] S. Kanai *et al.*, "Magnetization switching in a CoFeB/MgO magnetic tunnel junction by combining spin-transfer torque and electric field-effect," *Appl. Phys. Lett.*, vol. 104, no. 21, pp. 212406.1–212406.3, May 2014.

[3] H. Kubota *et al.*, "Evaluation of spin-transfer switching in CoFeB/MgO/CoFeB magnetic tunnel junctions," *Jpn. J. Appl. Phys.*, vol. 44, nos. 37–41, pp. L1237–L1240, Sep. 2005.

[4] X. Yao, J. Harms, A. Lyle, F. Ebrahimi, Y. Zhang, and J.-P. Wang, "Magnetic tunnel junction-based spintronic logic units operated by spin transfer torque," *IEEE Trans. Nanotechnol.*, vol. 11, no. 1, pp. 120–126, Jan. 2012.

[5] Z. Zeng *et al.*, "Ultralow-current-density and bias-field-free spin-transfer nano-oscillator," *Sci. Rep.*, vol. 3, Mar. 2013, Art. ID 1426.

[6] D. C. Ralph and M. D. Stiles, "Spin transfer torques," *J. Magn. Magn. Mater.*, vol. 320, no. 7, pp. 1190–1216, Dec. 2007.

[7] P. Gambardella and I. M. Miron, "Current-induced spin–orbit torques," *Philos. Trans. Roy. Soc. A*, vol. 369, no. 1948, pp. 3175–3197, Jul. 2011.

[8] I. M. Miron *et al.*, "Perpendicular switching of a single ferromagnetic layer induced by in-plane current injection," *Nature*, vol. 476, no. 7359, pp. 189–193, Aug. 2011.

[9] L. Liu, O. J. Lee, T. J. Gudmundsen, D. C. Ralph, and R. A. Buhrman, "Current-induced switching of perpendicularly magnetized magnetic layers using spin torque from the spin Hall effect," *Phys. Rev. Lett.*, vol. 109, p. 096602, Aug. 2012.

[10] L. Liu, C.-F. Pai, Y. Li, H. W. Tseng, D. C. Ralph, and R. A. Buhrman, "Spin-torque switching with the giant spin Hall effect of tantalum," *Science*, vol. 336, no. 6081, pp. 555–558, May 2012.

[11] M. Kazemi, E. Ipek, and E. G. Friedman, "Adaptive compact magnetic tunnel junction model," *IEEE Trans. Electron Devices*, vol. 61, no. 11, pp. 3883–3891, Nov. 2014.

[12] K. Jabeur, G. Di Pendina, G. Prenat, L. D. Buda-Prejbeanu, and B. Dieny, "Compact modeling of a magnetic tunnel junction based on spin orbit torque," *IEEE Trans. Magn.*, vol. 50, no. 7, Jul. 2014, Art. ID 4100208.

[13] K. Jabeur, G. Prenat, G. Di Pendina, L. D. Buda-Prejbeanu, I. L. Prejbeanu, and B. Dieny, "Compact model of a three-terminal MRAM device based on spin orbit torque switching," in *Proc. Int. Semiconductor Conf.*, Sep. 2013, pp. 1–4.

[14] S.-C. Oh *et al.*, "Bias-voltage dependence of perpendicular spin-transfer torque in asymmetric MgO-based magnetic tunnel junctions," *Nature Phys.*, vol. 5, pp. 898–902, Oct. 2009.

[15] O. J. Lee *et al.*, "Central role of domain wall depinning for perpendicular magnetization switching driven by spin torque from the spin Hall effect," *Phys. Rev. B*, vol. 89, pp. 024418-1–024418-8, Jan. 2014.

[16] J. Kim *et al.*, "Layer thickness dependence of the current-induced effective field vector in Ta|CoFeB|MgO," *Nature Mater.*, vol. 12, pp. 240–245, Dec. 2012.

[17] D. Fitzpatrick and I. Miller, *Analog Behavioral Modeling With the Verilog-A Language*. Kluwer, 1998.

[18] J. C. Slonczewski, "Current-driven excitation of magnetic multilayers," *J. Magn. Magn. Mater.*, vol. 159, nos. 1–2, pp. L1–L7, Jun. 1996.

[19] W. F. Brown, Jr., "Thermal fluctuations of a single-domain particle," *Phys. Rev.*, vol. 130, no. 5, pp. 1677–1686, Jun. 1963.

[20] J. Z. Sun, "Spin angular momentum transfer in current-perpendicular nanomagnetic junctions," *IBM J. Res. Develop.*, vol. 50, no. 1, pp. 81–100, Jan. 2006.

[21] G. D. Panagopoulos, C. Augustine, and K. Roy, "Physics-based SPICE-compatible compact model for simulating hybrid MTJ/CMOS circuits," *IEEE Trans. Electron Devices*, vol. 60, no. 9, pp. 2808–2814, Sep. 2013.

[22] J. Park, G. E. Rowlands, O. J. Lee, D. C. Ralph, and R. A. Buhrman, "Macrospin modeling of sub-ns pulse switching of perpendicularly magnetized free layer via spin-orbit torques for cryogenic memory applications," *Appl. Phys. Lett.*, vol. 105, no. 10, pp. 102404-1–102404-5, Sep. 2014.

[23] E. Barati, M. Cinal, D. M. Edwards, and A. Umerski, "Gilbert damping in magnetic layered systems," *Phys. Rev. B*, vol. 90, pp. 014420-1–014420-16, Jul. 2014.

[24] J. Z. Sun, "Spin-current interaction with a monodomain magnetic body: A model study," *Phys. Rev. B*, vol. 62, no. 1, pp. 570–578, Jul. 2000.

[25] E. Salman and E. G. Friedman, *High Performance Integrated Circuit Design*. New York, NY, USA: McGraw-Hill, 2012.

[26] M. Jullière, "Tunneling between ferromagnetic films," *Phys. Lett. A*, vol. 54, no. 3, pp. 225–226, Sep. 1975.

[27] J. C. Slonczewski, "Conductance and exchange coupling of two ferromagnets separated by a tunneling barrier," *Phys. Rev. B*, vol. 39, pp. 6995–7002, Apr. 1989.

[28] W. F. Brinkman, R. C. Dynes, and J. M. Rowell, "Tunneling conductance of asymmetrical barriers," *Appl. Phys. Lett.*, vol. 41, no. 5, pp. 1915–1921, Jan. 1970.

[29] R. Stratton, "The influence of interelectronic collisions on conduction and breakdown in polar crystals," *Proc. R. Soc. Lond. A, Math. Phys. Sci.*, vol. 246, no. 1246, pp. 406–422, Aug. 1958.

[30] (Feb. 2014). *IMEC N14 FinFET Compact Model v0.3.0b*. [Online]. Available: http://www2.imec.be/

[31] K. Jabeur, G. Di Pendina, F. Bernard-Granger, and G. Prenat, "Spin orbit torque non-volatile flip-flop for high speed and low energy applications," *IEEE Electron Device Lett.*, vol. 35, no. 3, pp. 408–410, Mar. 2014.

[32] Z. Wang, W. Zhao, E. Deng, J.-O. Klein, and C. Chappert, "Perpendicular-anisotropy magnetic tunnel junction switched by spin-Hall-assisted spin-transfer torque," *J. Phys. D, Appl. Phys.*, vol. 48, no. 6, pp. 065001-1–065001-7, Jan. 2015.

[33] Y. Zhang *et al.*, "Compact modeling of perpendicular-anisotropy CoFeB/MgO magnetic tunnel junctions," *IEEE Trans. Electron Devices*, vol. 59, no. 3, pp. 819–826, Mar. 2012.

[34] M. Kazemi, E. Ipek, and E. G. Friedman, "Energy-efficient nonvolatile flip-flop with subnanosecond data backup time for fine-grain power gating," *IEEE Trans. Circuits Syst. II, Exp. Briefs*, vol. 62, no. 12, pp. 1154–1158, Dec. 2015.

Mohammad Kazemi (S'10) received the B.Sc. degree in electronics from the University of Shahrekord, in 2007, and the M.Sc. degree in electrical engineering from the K. N. Toosi University of Technology, in 2010.

He is currently conducting a research on spin orbitronics nanostructures with application in beyond Von Neumann computation and high frequency signal generation.

Graham E. Rowlands received the B.A. degree in physics from Boston University, Boston, MA, USA, in 2007, and the Ph.D. degree in physics from the University of California at Irvine, Irvine, CA, USA, in 2012.

He held a post-doctoral position with Cornell University, Ithaca, NY, USA. He joined Raytheon BBN Technologies, Cambridge, MA, USA, in 2015, where he is continuing to investigate the interoperation of magnetic RAM with cryogenic superconducting computing schemes.

Engin Ipek (M'09) received the Ph.D. degree in electrical and computer engineering from Cornell University, Ithaca, NY, USA, in 2008.

He is currently an Associate Professor of Electrical and Computer Engineering and Computer Science with the University of Rochester, Rochester, NY, USA.

Robert A. Buhrman has been a member with Cornell University, Ithaca, NY, USA, since 1973, where he is currently the John Edson Sweet Professor with the School of Applied and Engineering Physics. His current research interests include applied condensed matter physics and nanoscale science and engineering with a current focus on nanomagnetic materials and spintronics devices.

Eby G. Friedman (F'00) is a Distinguished Professor with the University of Rochester, Rochester, NY, USA, and a Visiting Professor with the Technion—Israel Institute of Technology. He is the author of almost 500 papers, book chapters, and patents, and 17 books in the fields of high speed and low power CMOS circuits, 3-D integration, and synchronous clock and power delivery.

Dr. Friedman is a Senior Fulbright Fellow.